small
NANO MICRO

Hydrothermal Transformation of Dried Grass into Graphitic Carbon-Based High Performance Electrocatalyst for Oxygen Reduction Reaction

*Haimin Zhang, Yun Wang, Dan Wang, Yibing Li, Xiaolu Liu, Porun Liu, Huagui Yang, Taicheng An, Zhiyong Tang, and Huijun Zhao**

In this work, we present a low cost and environmentally benign hydrothermal method using dried grass as the sole starting material without any synthetic chemicals to directly produce high quality nitrogen-doped carbon nanodot/nanosheet aggregates (N-CNAs), achieving a high yield of 25.2%. The fabricated N-CNAs possess an N/C atomic ratio of 3.41%, consist of three typed of doped N at a ratio of 2.6 (pyridinic):1.7 (pyrrolic):1 (graphitic). The experimental results reveal that for oxygen reduction reaction (ORR), the performance of N-CNAs, in terms of electrocatalytic activity, stability and resistance to crossover effects, is better or comparable to the commercial Pt/C electrocatalyst. The theoretical studies further indicate that the doped pyridinic-N plays a key role for N-CNAs' excellent four-electron ORR electrocatalytic activity.

Dr. H. M. Zhang, Dr. Y. Wang, Y. B. Li, X. L. Liu,
Dr. P. R. Liu, Dr. A/Prof. H. G. Yang, Dr. Prof. H. J. Zhao
Centre for Clean Environment and Energy
Griffith University
Gold Coast Campus, QLD 4222, Australia
E-mail: h.zhao@griffith.edu.au

Dr. Prof. H. J. Zhao
Centre for Environmental and Energy Nanomaterials
Institutes of Solid State Physics
Chinese Academy of Sciences
Hefei 230031, China

Dr. Prof. D. Wang
State Key Laboratory of Multiphase Complex Systems
Institute of Process Engineering
Chinese Academy of Sciences
Beijing 100190, China

Dr. Prof. T. C. An
State Key Laboratory of Organic Geochemistry
Guangzhou Institute of Geochemistry
Chinese Academy of Sciences
Guangzhou 510640, China

Dr. Prof. Z. Y. Tang
Laboratory for Nanomaterials
National Center for Nanoscience and Technology
Beijing 100190, China

DOI: 10.1002/smll.201400781

1. Introduction

Fuel cells are the most promising clean energy generation devices for which electrocatalysts play a key role for the oxygen reduction half reaction (ORR). To date, the reported high performance fuel cells almost exclusively employ the Pt-based electrocatalysts.[1–3] Although Pt-based materials have been the most effective ORR electrocatalysts, it is generally accepted that the large-scale production and application of fuel cells using Pt-based electrocatalysts are not commercially viable because of the high cost and the scarcity of Pt. Therefore, the development of high efficiency, cheap and earth-abundant ORR electrocatalysts to replace Pt-based electrocatalysts is paramount for the future of the fuel cell technology.[4–13]

To date, amongst varieties of investigated metal-free ORR electrocatalysts, heteroatom-doped carbon materials are widely recognized as a class of promising candidates.[6,8–12,14–21] Theoretical and experimental studies have revealed that the doping of heteroatom (*e.g.,* N, B, S, P) leads to its adjacent carbon atoms being positively cha rged.[6,8,12,14,17,20–24] Such changes in charge distribution facilitate oxygen adsorption at the catalyst surface to reduce the ORR overpotential, enhancing the electrocatalytic

© 2014 Wiley-VCH Verlag GmbH & Co. KGaA, Weinheim

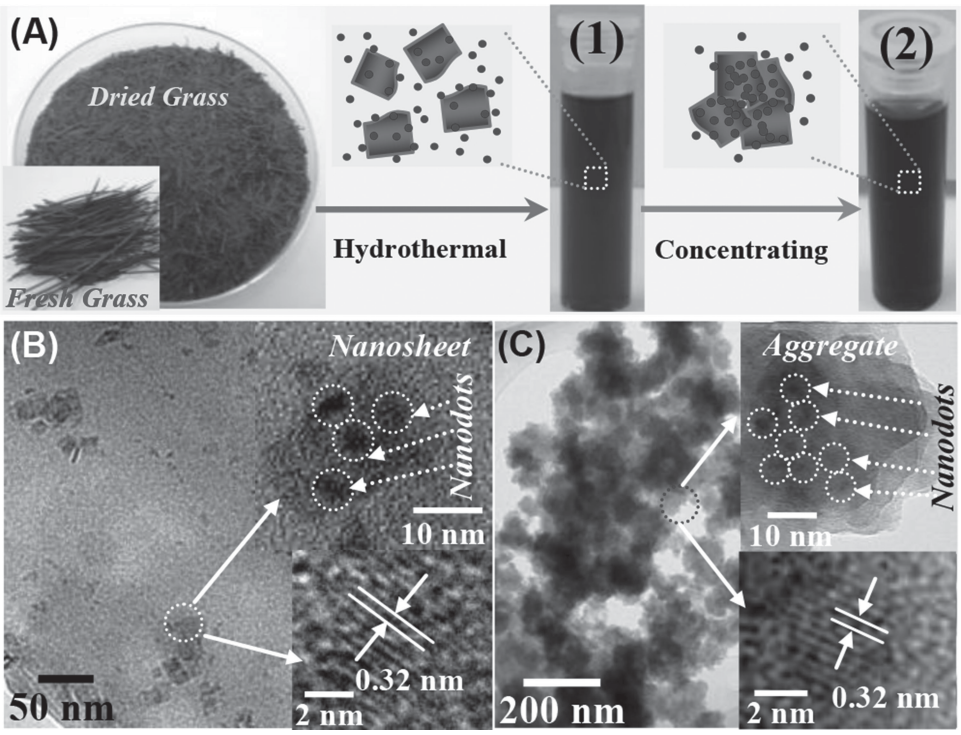

Figure 1. (A) Fabrication procedure of the N-CNs and N-CNAs. (B) and (C) TEM images of the N-CNs and N-CNAs; insets are corresponding high magnification TEM and HRTEM images.

activity.[6,8,12,14,17,22,23] Various approaches have been employed to dope heteroatoms into carbon structures (*e.g.,* high temperature carbonization of heteroatom-contained precursors, high temperature post treatment, electrochemical method, liquid phase polymerization, and hydrothermal treatment of heteroatom-contained precursors).[6,8,11,12,14,15,17–19,23,25] However, these approaches either involve tedious and complex experimental procedures or use harsh reaction conditions, or possess low yield production, and almost exclusively require the use of synthetic chemicals as carbon and heteroatom sources.[6,8,11,12,14,15,17–19,23,25] It is therefore highly desirable to realize heteroatom doping by simple, low cost and high yield green synthesis methods for fabrication of commercially viable carbon-based materials to replace Pt-based electrocatalysts for the ORR. The biomasses are a class of ideal starting materials for green synthesis of carbon materials because they are earth-abundant, readily available and cheap to obtain.[26–35] Biomasses and their derivatives are nitrogen containing materials that can be used to produce N-containing carbon materials.[27,28,30–34] In this regard, the majority of the reported works employ the biomass derivatives to produce N-containing carbon materials,[26–28,30–33] only few reports directly utilize the crude biomasses (*e.g.,* grass, soy milk and soy bean) to produce N-containing carbon materials,[16,34,35] due to the lack of satisfactory synthetic method for the production of valuable carbon materials.[28] Recently, N-doped carbon nanodots have been successfully fabricated under hydrothermal conditions using grass as precursor and used for analytical determination of heavy metal and iodide ions in water, demonstrating a feasibility of using crude biomass to produce valuable carbon materials.[35,36]

Herein, we report the fabrication of N-doped carbon nanodot/nanosheet aggregates (N-CNAs) using Monkey Grass as the sole material source *via* a simply hydrothermal process to achieve a high yield of 25.2% graphitic carbon production. The Monkey Grass was chosen because it is readily available, easier handling and processing. The synthesized N-CNAs possess an N/C atomic ratio of 3.41%, exhibit comparable stability and ORR electrocatalytic activity to those of reported carbon-based and commercial Pt/C electrocatalysts.[14–18] Although N-doped carbon nanodots fabricated by hydrothermal treatment of grass have been investigated for analytical determination of Cu^{2+} and iodide (I^-),[35,36] to the best of our knowledge, this is the first time a simply hydrothermal method is successfully used to achieve high yield production of high performance N-doped carbon-based ORR electrocatalyst using grass as the sole material source.

2. Results and Discussion

2.1. Structure and Composition

Hydrothermally treating dried grass at 180 °C for 10 h yielded a brown colored N-doped carbon nanodot/nanosheet solution (N-CNs) with a concentration of 21 mg mL^{-1} (photo (1) in **Figure 1**A). The mass yield of N-CNs is *ca.* 25.2%, which is significantly higher than that of carbon nanodot-based materials fabricated by other methods.[14,15,37] The concentrated solution *via* evaporation resulted in a dark brown colored solution containing 52 mg mL^{-1} N-doped carbon nanodot/nanosheet aggregates (N-CNAs) (photo (2) in Figure 1A). Detailed characterizations confirm that the as-synthesized N-CNs (Figure 1B) in the diluted solution were self-assembled

 © 2014 Wiley-VCH Verlag GmbH & Co. KGaA, Weinheim

into N-CNAs in the concentrated solution (Figure 1C). As shown in Figure 1B, the transmission electron microscopy (TEM) image of the diluted solution is a mixture of 2–6 nm nanodots and 10–50 nm nanosheets (top inset in Figure 1B). The high resolution TEM image of the resultant nanodot shows a lattice spacing of *ca*. 0.32 nm (bottom inset in Figure 1B), which is in agreement with the <002> spacing of graphitic carbon.[38] This can be further confirmed by X-ray diffraction (XRD) results (Figure S1, Supporting Information). Shown in Figure 1C is TEM image of the N-CNAs in the concentrated solution. These aggregates display a particle-like shape, assembled by aggregating the nanodots anchored nanosheets (top inset in Figure 1C). TEM image indicates uniformly dispersed nanodots on the nanosheet aggregates (top inset in Figure 1C), having a graphitic carbon lattice spacing of *ca*. 0.32 nm (bottom inset in Figure 1C), suggesting that the aggregation occurred during the concentrating process under low temperature evaporation only changes the size and shape of the products rather than their graphitic structures. Many studies have demonstrated that carbon materials synthesized by hydrothermal methods possess oxygen-rich surface functional groups, which may play a key role to facilitate the self-assembly aggregation during the concentrating process.[14,35,37,39]

Figure 2A shows XPS survey spectra of the N-CNs and N-CNAs, confirming the presence of C, N and O elements with similar N/C atomic ratios of 3.37% and 3.41%, respectively. Similar N/C ratios observed from N-CNs and N-CNAs further indicate that no significant graphitic structure changes occurred during the aggregation process. The high resolution C 1s spectrum of the N-CNAs (Figure 2B) indicates the existence of functional groups such as C–C (284.4 eV), C–N (285.2 eV), C–O (286.6 eV), and C = O (288.3 eV), confirming the presence of doped N and O-rich functional groups.[14,35] The high resolution N 1s spectrum of the N-CNAs (Figure 2C) reveals the presence of three types of N atoms, namely, pyridinic-N (398.9 eV), pyrrolic-N (399.8 eV) and graphitic-N (401.2 eV).[10] The relative atomic ratios of the three types of N in N-CNAs was found to be 2.6 (pyridinic):1.7 (pyrrolic):1 (graphitic). The C 1s and N 1s spectra of N-CNs reveal very similar findings (Figure S2, Supporting Information). Figure 2D shows FT-IR spectra of the as-synthesized N-CNs and N-CNAs samples. After concentrating at 70 °C, the obtained N-CNAs exhibit very similar FT-IR spectra with the N-CNs. This indicates that the surface functional groups of the N-CNAs remain the same before and after preconcentration via evaporation. Both the N-CNs and N-CNAs exhibit characteristic absorption bands of O–H and N–H stretching vibrations at 3404 and 3285 cm^{-1}, and C–H stretching vibration at 2934 cm^{-1}.[35,40] The characteristic absorption bands of aromatic CN heterocycles at 1280 to 1605 cm^{-1} were also observed, implying that the local structure of these carbon materials is consisted of CN units.[35] These FT-IR data are in an agreement with XPS analysis. It has been a consensus that N doping into carbon structures can lead to significantly enhanced ORR performance.[6,8,10,12,14,24] However, the relationship between the ORR electrocatalytic activity and the doped N types is still unclear and sometimes controversial,[6,22,41] which deserves a clarification.

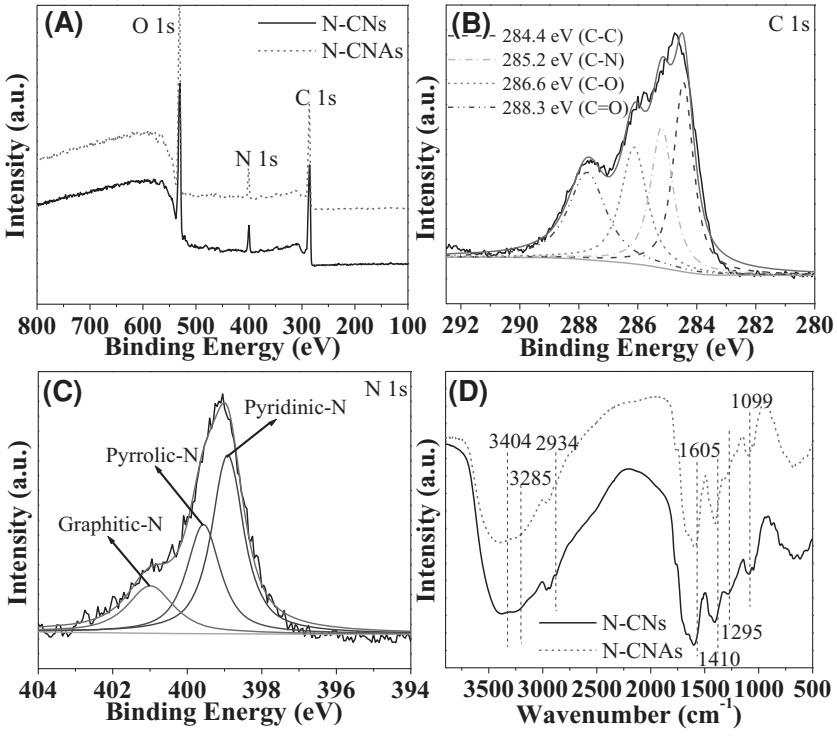

Figure 2. (A) XPS survey spectra of the N-CNs and N-CNAs. (B) and (C) High resolution XPS spectra of C 1s and N 1s of N-CNAs. (D) FT-IR spectra of the fabricated N-CNs and N-CNAs samples.

2.2. Optical Properties

N-doping improves the oxygen adsorption at the catalyst surface, which is one of the proposed ORR electrocatalytic activity enhancement mechanisms.[6,14,17] An experimental demonstration of surface oxygen adsorption would provide evidence to support such a speculation. It is known that the dissolved O_2 can be detected via a fluorescent quenching concept.[42,43] It is also known that carbon nanodots possess photoluminescence (PL) properties.[27,37] These could be used to our advantage to investigate the surface oxygen adsorption properties. The measured PL emission spectra are peaked at 450 nm and 485 nm for N-CNs and N-CNAs, respectively (**Figure 3**A). The red-shifted PL emission peak position of N-CNAs could be due to the size-dependent trap sites.[39,44] The effect of dissolved O_2 concentration on N-CNAs' PL intensity is shown in Figure 3B. The measured decrease in PL intensity as O_2 concentration increased is due to the quenching effect occurred at the surface of N-CNAs. Similar phenomenon can also be

 © 2014 Wiley-VCH Verlag GmbH & Co. KGaA, Weinheim

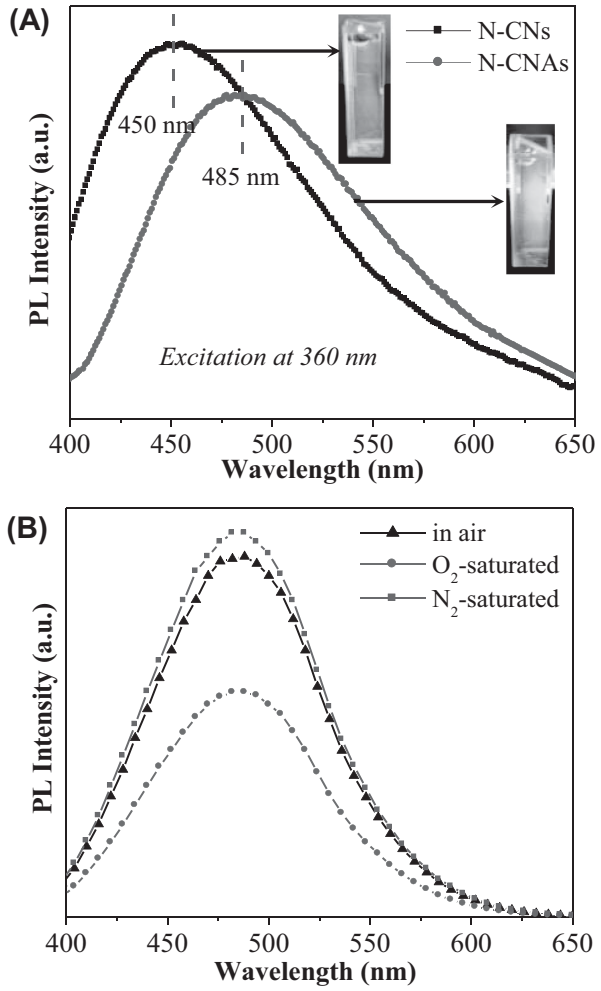

Figure 3. (A) PL spectra of the N-CNs and N-CNAs in water with excitation wavelength of 360 nm; the insets are the photos of the N-CNs and N-CNAs aqueous solutions under 365 nm UV illumination. (B) PL spectra of the N-CNAs aqueous solutions with air, O_2-saturated, and N_2-saturated situations. Excitation wavelength of 360 nm.

observed from N-CNs (Figure S3, Supporting Information). This is a direct evidence of strong O_2 interaction with the surface of N-doped carbon material, implying a strong O_2 adsorption at the surface of N-CNAs, beneficial for electrocatalytic ORR. In addition, the UV-vis absorption spectra of the N-CNs and N-CNAs indicate that the absorption bands of both materials are located at around 270 nm, consistent with the reported results (Figure S4, Supporting Information).[14,35] The absorption band edge of the N-CNAs is slightly red-shifted when compared to that of the N-CNs, further confirming the formation of large sized aggregates (Figure S4, Supporting Information).[45]

2.3. ORR Performance

The above results indicate that the obtained N-CNAs possess the required characteristics for a high performance carbon-based ORR electrocatalyst.[6,8,10,12,14–16] Electrocatalytic ORR performances of the N-CNAs were subsequently evaluated. To make the evaluation meaningful and comparative, where appropriate, the measurements of bare glassy carbon (GC) and N-CNs coated GC electrodes are performed under identical conditions as that for the N-CNAs coated GC electrode. Figure S5A (Supporting Information) shows the cyclic voltammetric (CV) responses of a bare GC electrode in 0.1 M KOH solutions saturated with N_2 or O_2. The CV curve obtained from the O_2-saturated solution exhibits distinctive characteristics for a two-electron transfer process (reducing O_2 to H_2O_2) with a cathodic current peak at *ca.* –0.44 V.[18,46] The CV curve obtained from N-CNs coated GC electrode reveals similar characteristics as that of the bare GC electrode, with an increased cathodic current and slightly positively shifted peak potential to *ca.* –0.42 V (Figure S5B, Supporting Information). Although the electrocatalytic activity of N-CNs is observable, the process is dominated by a two-electron transfer reduction process.[12,18,46] A careful investigation revealed that the measured response is largely contributed by the bare GC rather than N-CNs.[14] This is due to the difficulties to form a uniform and stable N-CNs film that completely covers the GC substrate and the formed film easily felling off the substrate during the measurement (**Figure 4**B, E). Different immobilization approaches were hence attempted to improve the coverage, uniformity and stability of the coated film, but failed due to the extremely high water adsorption property of N-CNs. Similar issue has also been experienced by Qu and co-workers in their recent study on the N-doped graphene quantum dots (N-GQDs).[14] They failed to directly use the as-synthesized N-GQDs as ORR electrocatalyst because of the difficulties to form a stable and continuous N-GQD film onto GC electrode.[14] For carbon-based electrocatalysts, the coverage and stability of the catalyst film on the conducting substrate largely determine their applicability, but the key factors affecting the film quality are not yet understood. Available evidences to us suggest that the quality of the immobilized film is size dependent. A smaller size leads to a larger volume expansion after water adsorption, hence a deceased stability. To confirm this, we fabricated well dispersed pure N-doped carbon nanodots

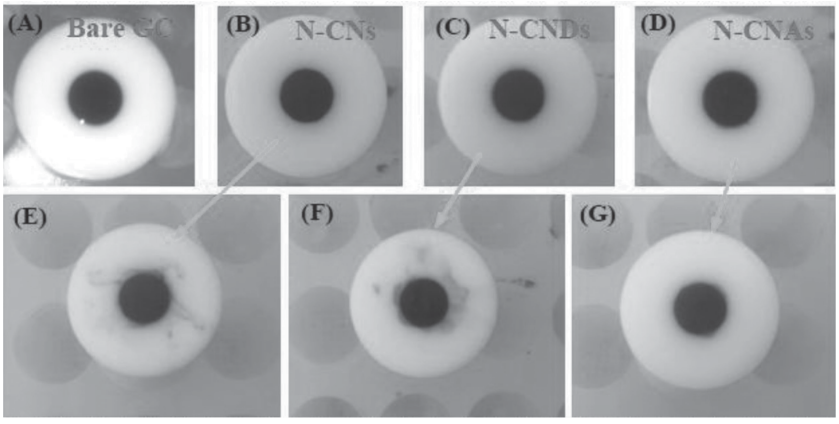

Figure 4. Photos of bare GC electrode (A) and N-CNs coated (B, E), N-CNDs coated (C, F) and N-CNAs coated (D, G) electrodes before and after electrocatalytic measurements.

© 2014 Wiley-VCH Verlag GmbH & Co. KGaA, Weinheim

NANO MICRO small

(N-CNDs, Figure S6, Supporting Information), that possess even higher hydration volume expansion than N-CNs. The cyclic voltammetric responses obtained from the N-CNDs coated GC electrode are found to be almost identical to that obtained from the bare GC electrode, because the immobilized N-CNDs film was rapidly displaced from GC surface (Figure 4C, F).[35] The above results suggest that to obtain high quality catalyst film, the size and the interactive force among the individual carbon structure unit and the substrate must be carefully managed. In this work, an appropriate degree of aggregation of N-CNs would be a viable means to increase the size and the interactive forces amongst the carbon materials and the substrate. For N-CNAs, the formed catalyst film onto GC can maintain high stability (*e.g.*, 20,000 s, Figure 4G), while the N-CNs and N-CNDs films quickly dissolve during measurement (*e.g.*, 2 min).

Figure 5A shows the cyclic voltammetric (CV) responses of the N-CNAs coated GC electrode in 0.1 M KOH solutions saturated with N_2 or O_2. The obtained O_2 reduction peak potential at *ca.* –0.21 V is very close to that of the commercial Pt/C electrocatalyst (*ca.* –0.18 V, Figure 5B) and 230 or 210 mV anodically shifted when compared to the bare GC or N-CNs coated GC electrodes, respectively (Figure S5A and B, Supporting Information). It is well known that a Pt/C electrocatalyst often suffered from the crossover effects of fuel molecules such as methanol (Figure 5B). In strong contrast, the N-CNAs electrocatalyst exhibits a superior resistance to the crossover effects (Figure 5A) in presence of 3 M methanol. Figure 5C shows the linear sweep voltammetric (LSV) responses of N-CNAs and Pt/C coated GC rotating disc electrodes (RDE) under a rotation rate of 1000 rpm. It was found that the N-CNAs and the commercial Pt/C electrocatalysts possess almost identical onset potential of –0.08 V, indicating an intrinsic characteristic of low overpotential for ORR. Similar to the commercial Pt/C electrocatalyst, a wide current plateau can be observed for N-CNAs within a wide potential range, highly desirable for a high performance electrocatalyst.[23] Moreover, the current density of the N-CNAs electrocatalyst resulting from ORR is comparable to that of the Pt/C electrocatalyst, indicating a superior electrocatalytic activity of the N-CNAs. The number of transferred electron (ideally, four electrons) involved in an ORR is an important parameter to evaluate the performance of an ORR electrocatalyst, which can be determined by Koutecky–Levich equations as follows:[6,11,14]

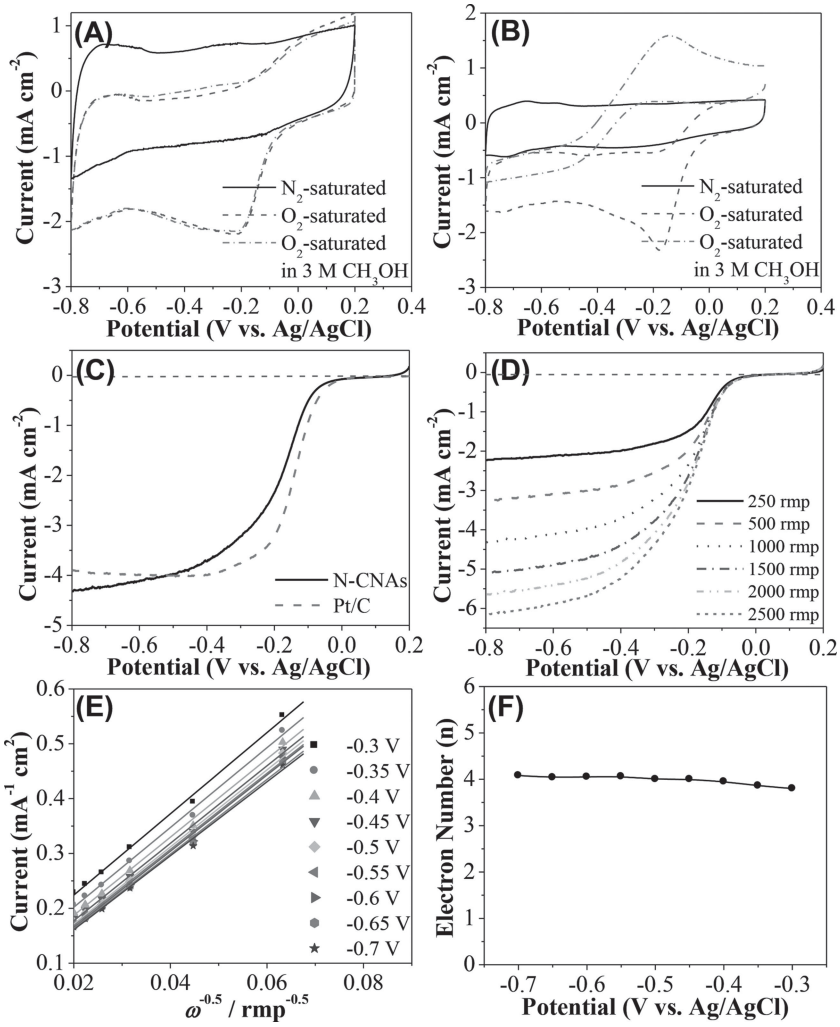

Figure 5. (A) and (B) CV responses of the N-CNAs and Pt/C electrocatalysts in N_2-saturated 0.1 M KOH, O_2-saturated 0.1 M KOH, and O_2-saturated 3 M methanol solutions. (C) LSV responses of N-CNAs and Pt/C electrocatalysts using a RDE at 1000 rpm and 10 mV s^{-1}. (D) LSV responses of N-CNAs in an O_2-saturated 0.1 M KOH solution measured on a RDE for different rotation rates. (E) Koutecky-Levich plots derived from the RDE measurements for N-CNAs. (F) The dependence of electron transfer number on the potential (the data were derived from Figure 5E).

$$\frac{1}{J}=\frac{1}{J_L}+\frac{1}{J_K}=\frac{1}{B\varpi^{1/2}}+\frac{1}{J_K} \quad (1)$$

where J is the measured current density, J_L and J_K are the diffusion limiting and kinetic current densities, respectively. ω is the angular velocity of the disk ($\omega = 2\pi N$, N is the linear rotation speed). B is Levich slope that is expressed by:

$$B = 0.2nFC_0(D_0)^{2/3}\nu^{-1/6} \quad (2)$$

where n is the overall number of electrons transferred in a oxygen reduction process. Based on Eqs. (1) and (2), the transferred electron number (n) and J_K can be obtained from the slope and intercept of the Koutecky-Levich plots, respectively. F is the Faraday constant (F = 96485 C mol^{-1}), C_0 is the bulk concentration of O_2 in electrolyte solution ($C_0 = 1.2 \times 10^{-3}$ mol L^{-1}), ν is the kinetic viscosity of the electrolyte (ν = 0.01 cm^2 s^{-1} in 0.1 M KOH). D_0 is the diffusion coefficient of O_2 in 0.1 M KOH ($D_0 = 1.9 \times 10^{-5}$ cm^2 s^{-1}). A

 © 2014 Wiley-VCH Verlag GmbH & Co. KGaA, Weinheim

constant value of 0.2 is adopted when the rotating speed is expressed in rpm.

Figure 5D shows the LSV curves of the N-CNAs coated GC obtained from an O_2-saturated 0.1 M KOH solution under different rotation rates. An increase in the rotation rate leads to an increase in the cathodic current, indicating a mass transfer controlled process.[20] Based on Figure 5D, the corresponding Koutecky-Levich curves were plotted for various potentials, as shown in Figure 5E. The excellent linear relationships for all plots obtained under various rotation rates for the potential range investigated suggest a first-order reaction with a respect to the dissolved O_2. The transferred electron number per O_2 molecule involved in the ORR process can be determined by the slope and intercept of the Koutecky–Levich plots as shown in Figure 5E. The transferred electron number (n) for the N-CNAs calculated from Figure 5E are found to be between 3.80 and 4.08 over the potential range of –0.3 V to –0.7 V (Figure 5F), implying a four-electron ORR process.[14,17] This is further validated by the negligible anodic current measured at a Pt ring of a rotating ring-disk electrode (Figure S7, Supporting Information). The operational stability is also an important parameter for an ORR electrocatalyst. As shown in Figure S8 (Supporting Information), the stability test indicates that the N-CNAs exhibit only 5.5% decrease in current density over 20,000 s of continuous operation at a rotation rate of 1000 rpm, under an applied potential of –0.4 V, whereas almost 27% decrease in current density was observed from the Pt/C, suggesting the N-CNAs possess a superior operational stability over the commercial Pt/C electrocatalyst.

It has been accepted that doping N into carbon materials creates electrocatalytic active sites.[6,10] However, the effect of doped N types on ORR electrocatalytic activity remains unclear. A better understanding of the issue will benefit future design and development of such type of electrocatalysts. In this work, three identified N-doped types (pyridinic-N, pyrrolic-N and graphitic-N) in N-CNAs are investigated using density functional theory (DFT) calculations. The DFT calculations indicate that the doped N atom is highly negatively charged (*ca.* –2.70), regardless of doped N types (Figure S9, Supporting Information). Compared to pyrrolic-N and graphitic-N, the carbon atoms around pyridinic-N possess higher positive charge (+1.21), beneficial to improving O_2 adsorption at the catalyst, hence the ORR performance.[6] The DFT calculations in this work further confirm that O_2 adsorption for pyridinic-N (ΔE_{ad} = –0.82 eV) is stronger than that for pyrrolic-N (ΔE_{ad} = –0.05 eV) and graphitic-N (ΔE_{ad} = –0.15 eV), indicating a better ORR catalytic activity of the pyridinic-N (Figure S10, Supporting Information). The calculated charge distribution indicates that the carbon atoms around pyridinic-N possess more positive charges and stronger O_2 adsorption. The experimentally confirmed four-electron ORR process at N-CNAs could be due to the mechanism of dissociative adsorption of O_2 molecules.[10] Our theoretical calculations reveal that pyridinic-N and pyrrolic-N exhibit stronger dissociative adsorption (ΔE_{dis} = –2.69 eV for pyridinic-N and ΔE_{dis} = –3.02 eV for pyrrolic-N), while the dissociative adsorption is energetically unfavorable for undoped carbon and graphitic-N products, as shown in **Figure 6**. Considering O_2 adsorption on electrocatalyst being first-step for the ORR, although pyrrolic-N has stronger dissociative adsorption than that of pyridinic-N, the relatively weak O_2 adsorption of pyrrolic-N makes pyridinic-N more efficient for the ORR, which is in agreement with our experimental results (pyridinic-N is dominant in N-CNAs by XPS analysis). In this work, we present only one possible situation of the influence of N doping species on the resulting ORR activity. The study on synergistic effect of three types of doped N species for the N-CNAs' performance may be more close to a real situation, which deserves a further investigation in the future.

3. Conclusion

In summary, we have demonstrated a facile and low cost hydrothermal method to produce high quality N-CNAs at a yield as high as 25.2%. This is an environmentally benign method using grass as the sole starting material without any synthetic chemicals. The obtained N-CNAs exhibit outstanding electrocatalytic activity, operational stability and high resistance to methanol crossover oxidation reaction. The theoretical studies indicate that the doped pyridinic-N plays an important role for N-CNAs' excellent four-electron ORR electrocatalytic activity. The concept validated in this work demonstrates the feasibility using biomass as the starting material to produce high quality and high performance carbon-based electrocatalysts in a high-yield, cost-effective and environmentally friendly manner.

4. Experimental Section

Synthesis: N-doped carbon nanodot/Nanosheet solution (N-CNs) was firstly prepared by a facile, one-step hydrothermal method using dried Monkey Grass (*Ophiopogon Japonicus*) as the sole starting material without any synthetic chemicals. In a typical preparation, fresh grass was firstly washed, and then dried at 100 °C for 10 h. The dried grass was subsequently ground into powder form and used as the starting material. The powder form dried grass (5.0 g) was mixed with 60 mL of deionized water. The mixture was then transferred into a 100 mL of Teflon lined autoclave and kept at 180 °C for 10 h. After hydrothermal reaction, the N-CNs was collected by centrifugation at 4500 rpm for 15 min to remove large size products. The concentration of the as-prepared N-CNs is *ca.* 21 mg mL^{-1}. The obtained N-CNs was preserved for further characterization and use. Pure N-doped carbon nanodods (N-CNDs) were obtained by centrifugation of the hydrothermal product at a centrifugal rate of 14 000 rpm for 20 min. N-doped carbon nanodot/nanosheet aggregates (N-CNAs) were obtained by evaporation of N-CNs solution at 70 °C for 6 h. The resulting N-CNAs (*ca.* 52 mg mL^{-1}) were collected and preserved for further characterization and use.

Measurements: All electrochemical measurements were carried out using a three-electrode system consisting of a working electrode, an Ag/AgCl reference electrode (3.0 M) and a platinum mesh counter electrode. CV measurements were carried out using a computer-controlled potentiostat (CHI 760D, CH Instruments, USA) in a standard three-electrode cell at a scan rate of 100 mV s^{-1}. Prior

 © 2014 Wiley-VCH Verlag GmbH & Co. KGaA, Weinheim

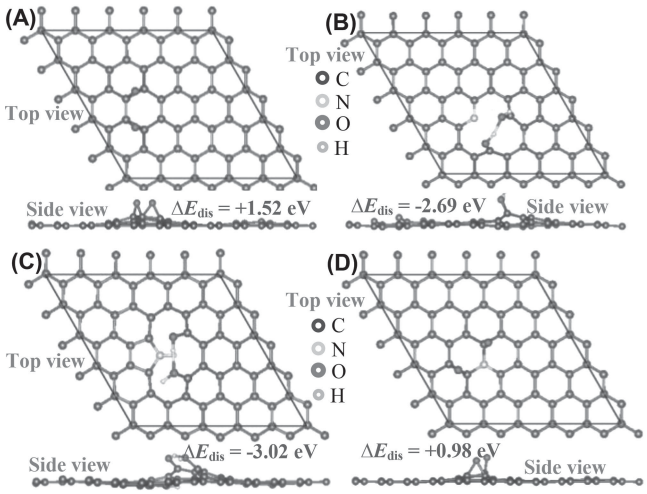

Figure 6. Dissociative adsorption energy (minus denotes exothermic reaction) in optimized structures. (A) Undoped carbon; (B) Pyridinic-N; (C) Pyrrolic-N; (D) Graphitic-N.

to measurements, RDE (GC, 5.0 mm in diameter, Pine Instrument) was firstly polished using 1.0, 0.3 and 0.05 μm alumina slurry sequentially, and then rinsed adequately using deionized water and ethanol in ultrasonic bath. The cleaned RDE was then dried in a N_2 stream for immobilization of N-CNDs, N-CNs, N-CNAs and commercial Pt/C (Vulcan, 20 wt. %) catalysts. 1.5 mg mL^{-1} N-CNDs, N-CNs, N-CNAs and Pt/C solutions (in 0.2% Nafion aqueous solutions) were firstly prepared. 10 μL of the prepared catalyst solution was cast on the cleaned RDE, then dried in air. Subsequently, another 5.0 μL of 1.0% Nafion aqueous solution was coated on the electrode surface, and dried at 60 °C. The loading amount of catalyst on the RDE was *ca.* 76 μg cm^{-2}. The catalyst coated GC electrode was placed in an electrochemical cell containing 60 mL of N-saturated or O-saturated 0.1 M KOH solution with or without 3 M methanol. All measurements were performed using RED or RRED (Pine Modulated Speed Rotator with CE Mark (Pine Instrument) controlled by a CHI 760D electrochemical potentiostat).

Characterization: TEM analysis was performed using a Philips F20 electron microscopy. XRD patterns were obtained using a Shimadzu XRD-6000 diffractometer, equipped with a graphite monochromator. Chemical compositions of the samples were analyzed using XPS (Kratos Axis ULTRA incorporating a 165 mm hemispherical electron energy analyzer). All binding energies were carefully aligned by reference to the C 1s peak (284.6 eV) arising from surface hydrocarbons or possible adventitious hydrocarbon. FT-IR spectra of the samples were analyzed by a Perkin Elmer spectrum 1000 FT-IR spectrophotometer using KBr pellets. PL spectra of the N-CNs and N-CNAs in water were recorded by a F7000 Fluorescence Spectrophotometer (Hitachi, Japan) with slit width of 0.5 mm. The excitation wavelength was 360 nm. UV-vis absorption spectra of the samples were recorded on a Varian Cary 4500.

Calculations: All computations are performed using the Vienna *ab initio* simulation package (VASP) based on all-electron projected augmented wave (PAW) method.[47–49] A plane-wave basis set is employed to expand the smooth part of wave functions with a kinetic energy cut-off of 500 eV. For the electron-electron exchange and correlation interactions, the functional of PBE,[49] a form of the general gradient approximation (GGA), is used throughout with the spin-polarization calculation. The Brillouin-zone integrations were performed using Monkhorst-Pack grids of special points, with gamma-point centered (4 × 4 × 1) *k*-points meshes used for the (5 × 5) graphene cell. When the geometry is optimized, all atoms are allowed to relax. And the geometric structures are optimized until the residual forces were below 0.001 eV/Å.

Supporting Information

Supporting Information is available from the Wiley Online Library or from the author.

Acknowledgements

This work was financially supported by Australian Research Council (ARC) Discovery Project and the Natural Science Foundation of China (Grant No. 51372248).

[1] J. Greeley, I. E. L. Stephens, A. S. Bondarenko, T. P. Johansson, H. A. Hansen, T. F. Jaramillo, J. Rossmeisl, I. Chorkendorff, J. K. Norskov, *Nat. Chem.* **2009**, *1*, 552.
[2] V. Di Noto, E. Negro, *Fuel Cell.* **2010**, *10*, 234.
[3] C. Wang, N. M. Markovic, V. R. Stamenkovic, *ACS Catal.* **2012**, *2*, 891.
[4] S. I. Shin, A. Go, I. Y. Kim, J. M. Lee, Y. Lee, S.-J. Hwang, *Energy Environ. Sci.* **2013**, *6*, 608.
[5] Y. Liang, Y. Li, H. Wang, J. Zhou, J. Wang, T. Regier, H. Dai, *Nature Mater.* **2011**, *10*, 780.
[6] K. Gong, F. Du, Z. Xia, M. Durstock, L. Dai, *Science* **2009**, *323*, 760.
[7] F. Jaouen, E. Proietti, M. Lefevre, R. Chenitz, J.-P. Dodelet, G. Wu, H. T. Chung, C. M. Johnston, P. Zelenay, *Energy Environ. Sci.* **2011**, *4*, 114.
[8] S. Wang, L. Zhang, Z. Xia, A. Roy, D. W. Chang, J.-B. Baek, L. Dai, *Angew. Chem., Int. Ed.* **2012**, *51*, 4209.
[9] Y. Sun, Q. Wu, G. Shi, *Energy Environ. Sci.* **2011**, *4*, 1113.
[10] H. Wang, T. Maiyalagan, X. Wang, *ACS Catal.* **2012**, *2*, 781.
[11] L. Qu, Y. Liu, J.-B. Baek, L. Dai, *ACS Nano* **2010**, *4*, 1321.
[12] S. Wang, E. Iyyamperumal, A. Roy, Y. Xue, D. Yu, L. Dai, *Angew. Chem., Int. Ed.* **2011**, *50*, 11756.
[13] Y. Zheng, Y. Jiao, M. Jaroniec, Y. Jin, S. Z. Qiao, *Small* **2012**, *8*, 3550.
[14] Y. Li, Y. Zhao, H. Cheng, Y. Hu, G. Shi, L. Dai, L. Qu, *J. Am. Chem. Soc.* **2012**, *134*, 15.
[15] Q. Li, S. Zhang, L. Dai, L.-s. Li, *J. Am. Chem. Soc.* **2012**, *134*, 18932.
[16] C. Zhu, J. Zhai, S. Dong, *Chem. Commun.* **2012**, *48*, 9367.
[17] J. Liang, Y. Jiao, M. Jaroniec, S. Z. Qiao, *Angew. Chem., Int. Ed.* **2012**, *51*, 11496.
[18] Z.-W. Liu, F. Peng, H.-J. Wang, H. Yu, W.-X. Zheng, J. Yang, *Angew. Chem., Int. Ed.* **2011**, *50*, 3257.
[19] C. H. Choi, M. W. Chung, H. C. Kwon, S. H. Park, S. I. Woo, *J. Mater. Chem. A* **2013**, *1*, 3694.
[20] R. Liu, D. Wu, X. Feng, K. Muellen, *Angew. Chem., Int. Ed.* **2010**, *49*, 2565.
[21] W. Yang, T.-P. Fellinger, M. Antonietti, *J. Am. Chem. Soc.* **2011**, *133*, 206.
[22] Z. Luo, S. Lim, Z. Tian, J. Shang, L. Lai, B. MacDonald, C. Fu, Z. Shen, T. Yu, J. Lin, *J. Mater. Chem.* **2011**, *21*, 8038.
[23] Y. Zheng, Y. Jiao, L. Ge, M. Jaroniec, S. Z. Qiao, *Angew. Chem., Int. Ed.* **2013**, *52*, 3110.

 © 2014 Wiley-VCH Verlag GmbH & Co. KGaA, Weinheim

[24] Z.-S. Wu, S. Yang, Y. Sun, K. Parvez, X. Feng, K. Muellen, *J. Am. Chem. Soc.* **2012**, *134*, 9082.
[25] F. L. Braghiroli, V. Fierro, M. T. Izquierdo, J. Parmentier, A. Pizzi, A. Celzard, *Carbon* **2012**, *50*, 5411.
[26] J. P. Paraknowitsch, A. Thomas, M. Antonietti, *Chem. Mater.* **2009**, *21*, 1170.
[27] S. N. Baker, G. A. Baker, *Angew. Chem., Int. Ed.* **2010**, *49*, 6726.
[28] B. Hu, K. Wang, L. Wu, S.-H. Yu, M. Antonietti, M.-M. Titirici, *Adv. Mater.* **2010**, *22*, 813.
[29] J. P. Paraknowitsch, A. Thomas, M. Antonietti, *ChemSusChem* **2010**, *3*, 223.
[30] A. Primo, P. Atienzar, E. Sanchez, J. M. Delgado, H. Garcia, *Chem. Commun.* **2012**, *48*, 9254.
[31] K. Wang, H. Wang, S. Ji, H. Feng, V. Linkov, R. Wang, *RSC Adv.* **2013**, *3*, 12039.
[32] R. J. White, M. Antonietti, M.-M. Titirici, *J. Mater. Chem.* **2009**, *19*, 8645.
[33] L. Zhao, N. Baccile, S. Gross, Y. Zhang, W. Wei, Y. Sun, M. Antonietti, M.-M. Titirici, *Carbon* **2010**, *48*, 3778.
[34] W. Li, Z. Yue, C. Wang, W. Zhang, G. Liu, *RSC Adv.* **2013**, *3*, 20662.
[35] S. Liu, J. Tian, L. Wang, Y. Zhang, X. Qin, Y. Luo, A. M. Asiri, A. O. Al-Youbi, X. Sun, *Adv. Mater.* **2012**, *24*, 2037.
[36] H. Zhang, Y. Li, X. Liu, P. Liu, Y. Wang, T. An, H. Yang, D. Jing, H. Zhao, *Environ. Sci. Technol. Lett.* **2014**, *1*, 87.
[37] H. Li, Z. Kang, Y. Liu, S.-T. Lee, *J. Mater. Chem.* **2012**, *47*, 24230.
[38] C. Wang, X. Wu, X. Li, W. Wang, L. Wang, M. Gu, Q. Li, *J. Mater. Chem.* **2012**, *22*, 15522.
[39] H. Li, X. He, Z. Kang, H. Huang, Y. Liu, J. Liu, S. Lian, A. Tsang Chi Him, X. Yang, S.-T. Lee, *Angew. Chem., Int. Ed.* **2010**, *49*, 4430.
[40] D. Hecht, L. Tadesse, L. Walters, *J. Am. Chem. Soc.* **1993**, *115*, 3336.
[41] D. Geng, Y. Chen, Y. Chen, Y. Li, R. Li, X. Sun, S. Ye, S. Knights, *Energy Environ. Sci.* **2011**, *4*, 760.
[42] M. Arik, N. Celebi, Y. Onganer, *J. Photochem. Photobiol., A Chem.* **2005**, *170*, 105.
[43] X. Xiong, D. Xiao, M. M. F. Choi, *Sens. Actuators, B Chem.* **2006**, *B117*, 172.
[44] M. J. Krysmann, A. Kelarakis, P. Dallas, E. P. Giannelis, *J. Am. Chem. Soc.* **2012**, *134*, 747.
[45] D. R. Baker, P. V. Kamat, *Adv. Funct. Mater.* **2009**, *19*, 805.
[46] T. Ohsaka, L. Mao, K. Arihara, T. Sotomura, *Electrochem. Commun.* **2004**, *6*, 273.
[47] G. Kresse, J. Hafner, *Phys. Rev. B* **1993**, *47*, 558.
[48] G. Kresse, J. Furthmller, *Comput. Mater. Sci.* **1996**, *6*, 15.
[49] G. Kresse, D. Joubert, *Phys. Rev. B* **1999**, *59*, 1758.

Received: March 23, 2014
Published online: April 14, 2014

 © 2014 Wiley-VCH Verlag GmbH & Co. KGaA, Weinheim